Activation Strain Model

International Edition: DOI: 10.1002/anie.201903196
German Edition: DOI: 10.1002/ange.201903196

# How Dihalogens Catalyze Michael Addition Reactions

*Trevor A. Hamlin, Israel Fernández,* and F. Matthias Bickelhaupt**

***Abstract:*** *We have quantum chemically analyzed the catalytic effect of dihalogen molecules ($X_2 = F_2$, $Cl_2$, $Br_2$, and $I_2$) on the aza-Michael addition of pyrrolidine and methyl acrylate using relativistic density functional theory and coupled-cluster theory. Our state-of-the-art computations reveal that activation barriers systematically decrease as one goes to heavier dihalogens, from 9.4 kcal mol$^{-1}$ for $F_2$ to 5.7 kcal mol$^{-1}$ for $I_2$. Activation strain and bonding analyses identify an unexpected physical factor that controls the computed reactivity trends, namely, Pauli repulsion between the nucleophile and Michael acceptor. Thus, dihalogens do not accelerate Michael additions by the commonly accepted mechanism of an enhanced donor–acceptor [HOMO(nucleophile)–LUMO(Michael acceptor)] interaction, but instead through a diminished Pauli repulsion between the lone-pair of the nucleophile and the Michael acceptor's π-electron system.*

The textbook Michael addition reaction, discovered by Arthur Michael in 1887,[1] constitutes one of the most useful and synthetically powerful tools in organic chemistry.[2] This is due to its ability to produce a new C–C bond in a single reaction step and with high or complete stereoselectivities (either diastereo- or enantioselectivity) when proper substrates and/or catalysts are used.[3] For this reason, this process, as well as its heteroatom variants (e.g. aza- or oxa-Michael additions), has been thoroughly applied toward the synthesis of a good number of target molecules including complex natural products[4] and compounds relevant in biochemistry.[5]

It is well known that dihalogen molecules ($X_2$), particularly molecular iodine, can be efficiently used as catalysts to significantly accelerate this fundamental reaction.[6] It is widely accepted that the origin of the catalytic effect of these species, in not only this but also in related transformations,[7] can be attributed to an attractive halogen bonding resulting from the interaction of the $X_2$ molecules and the substrate. This mode of activation strongly resembles that found in typical Lewis acid catalyzed processes, where the catalysis is mostly governed by a favorable interaction involving the corresponding frontier molecular orbitals (FMOs), namely HOMO(nucleophile)–LUMO(Michael acceptor).[8] Nevertheless, and despite recent studies on the mechanism of $I_2$-catalyzed Michael addition reactions,[9] very little is known about the ultimate factors behind the catalytic activity of $X_2$ molecules. For this reason, we decided to use state-of-the-art computational methods[10] to quantitatively unravel the nature of the catalytic power of these species.

To this end, we focused on the parent aza-Michael reaction involving pyrrolidine and methyl acrylate (Scheme 1), which was experimentally studied by Borah and co-workers.[6d] We considered both the uncatalyzed process and the analogous $X_2$-catalyzed reactions (where $X_2 = F_2$, $Cl_2$, $Br_2$, and $I_2$).

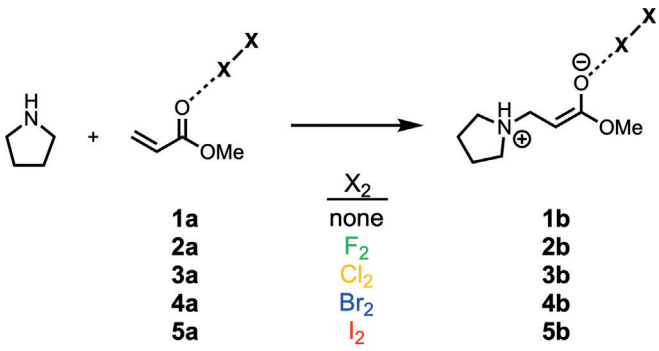


***Scheme 1.*** Computationally analyzed Michael addition reactions.

First, we analyzed the nature and strength of the interaction between $X_2$ and methyl acrylate in the initial methyl acrylate–$X_2$ reactants **2a**–**5a** using the energy decomposition analysis (EDA; see below) method (Table 1).[11] The complexation energies are nearly exclusively determined by the interaction energies, which are all stabilizing and become stronger when moving down Group 17, ranging from −1.4 to −5.6 kcal mol$^{-1}$ for **2a** to **5a**, respectively. The corresponding X···O distance becomes steadily longer in line with the increasing effective size of the halogen atom down Group 17. The electrostatic attractions are nearly twice as strong as the orbital interactions, which agrees with the electrostatic nature

[*] Dr. T. A. Hamlin, Prof. Dr. F. M. Bickelhaupt
Department of Theoretical Chemistry
Amsterdam Center for Multiscale Modeling (ACMM)
Vrije Universiteit Amsterdam
De Boelelaan 1083, 1081 HV Amsterdam (The Netherlands)
E-mail: f.m.bickelhaupt@vu.nl
Prof. Dr. I. Fernández
Departamento de Química Orgánica I and Centro de Innovación en Química Avanzada (ORFEO-CINQA), Facultad de Ciencias Química
Universidad Complutense de Madrid
28040 Madrid (Spain)
E-mail: israel@quim.ucm.es
Prof. Dr. F. M. Bickelhaupt
Institute for Molecules and Materials (IMM), Radboud University
Heyendaalseweg 135, 6525 AJ Nijmegen (The Netherlands)
Supporting information and the ORCID identification numbers for the authors of this article can be found under: https://doi.org/10.1002/anie.201903196.

***Table 1:*** Energy decomposition analysis terms (in kcal mol$^{-1}$) and X···O distance (in Å) computed on methyl acrylate–dihalogen adducts (**2a**–**5a**).[a]

| System | $\Delta E$ | $\Delta E_{strain}$ | $\Delta E_{int}$ | $\Delta E_{Pauli}$ | $\Delta V_{elstat}$ | $\Delta E_{oi}$ | $r$(X–X···O=C) |
|---|---|---|---|---|---|---|---|
| **2a**: $F_2$ | −1.4 | 0.0 | −1.4 | 1.3 | −1.8 | −0.9 | 2.701 |
| **3a**: $Cl_2$ | −3.4 | 0.0 | −3.4 | 4.7 | −5.5 | −2.6 | 2.745 |
| **4a**: $Br_2$ | −5.1 | 0.1 | −5.2 | 6.3 | −7.4 | −4.1 | 2.774 |
| **5a**: $I_2$ | −5.6 | 0.2 | −5.8 | 8.9 | −9.1 | −4.6 | 2.880 |

[a] The two interacting fragments are $X_2$ and methyl acrylate. Computed at the ZORA-M06-2X/TZ2P//M06-2X/def2-TZVP level.

of the X–X···O=C noncovalent interaction. Despite this, the orbital term is not negligible, which suggests that the FMOs of methyl acrylate are strongly affected by the dihalogen molecule, particularly for the heavier halogens (see below).

As seen from Table 2, the uncatalyzed reaction has the highest barrier (11.2 kcal mol$^{-1}$) and the least favorable reaction energy (−0.9 kcal mol$^{-1}$). Coordination of $X_2$ catalyst results in more favorable barrier heights that systematically

***Table 2:*** Energies (in kcal mol$^{-1}$) and key geometry details (in Å) computed on transition state structures for reactions 1–5. HOMO–LUMO energy gap (in eV) based on energy minima of pyrrolidine and **1a**–**5a**.[a]

| Reaction | $X_2$ | $\Delta E^{\neq}$ | $\Delta E_{rxn}$ | $\Delta\varepsilon$ $HOMO_{py}$–$LUMO_{1-5}$ | $r$(N···C)[b] |
|---|---|---|---|---|---|
| 1 | none | 11.2 (12.7) | −0.9 (0.2) | 7.4 | 1.829 |
| 2 | $F_2$ | 9.4 (11.7) | −1.3 (−0.4) | 7.2 | 1.847 |
| 3 | $Cl_2$ | 7.6 (9.7) | 1.7 (3.2) | 6.6 | 1.867 |
| 4 | $Br_2$ | 6.2 (8.1) | 0.9 (1.5) | 6.0 | 1.882 |
| 5 | $I_2$ | 5.7 (7.1) | 0.3 (0.4) | 5.8 | 1.883 |

[a] All data computed at the M06-2X/def2-TZVP level unless otherwise specified. Energies in parentheses were computed at the DLPNO-CCSD(T)/def2-TZVP//M06-2X/def2-TZVP level. [b] Forming bond length between the nucleophilic N(**py**) and the terminal olefinic carbon atom of methyl acrylate (**1a**–**5a**).

decrease when descending Group 17 for $X_2$, which is consistent with the experimental observations that bromine- and iodine-based halogen-bond donors are similarly active, whereas the corresponding chlorine derivatives are usually much less reactive.[9] The trend of our computed DFT barriers and reaction energies agrees well with those calculated at the DLPNO-CCSD(T)/def2-TZVP//M06-2X/def2-TZVP level. The corresponding transition states are reached earlier and earlier when going from the uncatalyzed to the $I_2$-catalyzed reaction (see N···C distance in Table 2) and this results in systematically lower and lower barrier heights. This is fully consistent with the Hammond–Leffer postulate.[12] For this reason, it is not surprising that a very good linear correlation is found when one plots the computed N···C bond-forming distances in the transition states vs. the activation barriers (correlation coefficient of 0.995, see Figure S1). Gibbs free energy barriers follow the same trend in reactivity as barriers computed using the electronic energy (Figure S2).

As mentioned above, the catalytic effect of dihalogen molecules has been typically attributed to the enhancement of the HOMO(nucleophile)–LUMO(Michael acceptor) interaction, where LUMO refers to the empty π* orbital of the Michael acceptor.[8] Figure 1 confirms that the computed electronic activation energies ($\Delta E^{\neq}$) correlate ($R^2 = 0.97$) with the $\Delta\varepsilon(HOMO_{py} \mid LUMO_{1a-5a})$ which, at first sight, seems to be in line with this traditional view on the origin of the computed reactivity trend.

We next turned to the activation strain model (ASM) of reactivity[13] to gain a deeper and quantitative insight into the

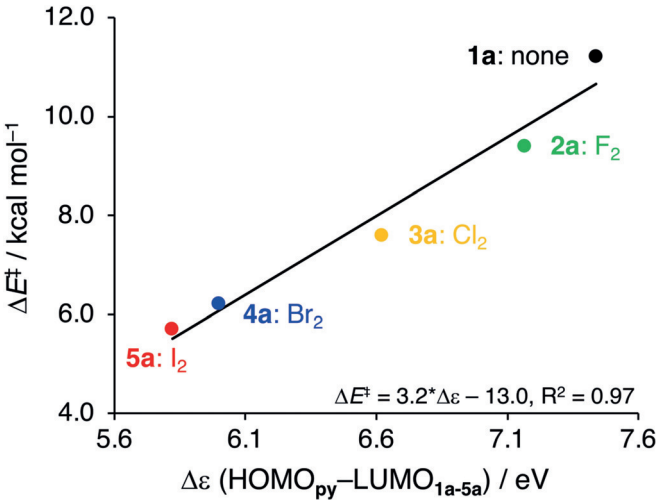


***Figure 1.*** Activation barriers for reactions of **1a**–**5a** with pyrrolidine (**py**) versus the reactants' $HOMO_{py}$–$LUMO_{1a-5a}$ gap $\Delta\varepsilon$, computed at the M06-2X/def2-TZVP level.

physical factors leading to the enhanced reactivity of $X_2$-catalyzed Michael addition reactions. This analysis decomposes the electronic energy ($\Delta E$) into two terms: the strain ($\Delta E_{strain}$) that results from the distortion of the individual reactants and the interaction ($\Delta E_{int}$) between the deformed reactants along the reaction coordinate, defined in this case by the C=C bond elongation in methyl acrylate. This geometrical parameter is critically involved in the reaction and undergoes a well-defined change over the course of the Michael addition.[14] Figure 2a shows the corresponding activation strain diagrams (ASDs) from the reactant complex to the transition states for the uncatalyzed (1) and $X_2$-catalyzed (2–5) Michael addition reactions. The accelerated reactivity of the $X_2$-catalyzed reactions originates primarily from a more stabilizing interaction energy along the entire reaction coordinate and also from a less destabilizing strain (albeit to a lesser extent). The interaction energy becomes increasingly more stabilizing in the order of $X_2$ = none < $F_2$ < $Cl_2$ < $Br_2$ < $I_2$ and this is exactly the same trend as the activation barriers. Thus, the reactivity trends is caused by the trend in the interaction between the two reactants. The strain energies for the $X_2$-catalyzed reactions are similar along the reaction coordinate but are less destabilizing compared to the uncatalyzed reaction.

Since the interaction energy plays such a critical role in the observed reactivity trends, the different contributors to the interaction energy were analyzed by applying our canonical energy decomposition analysis (EDA) which quantifies

  

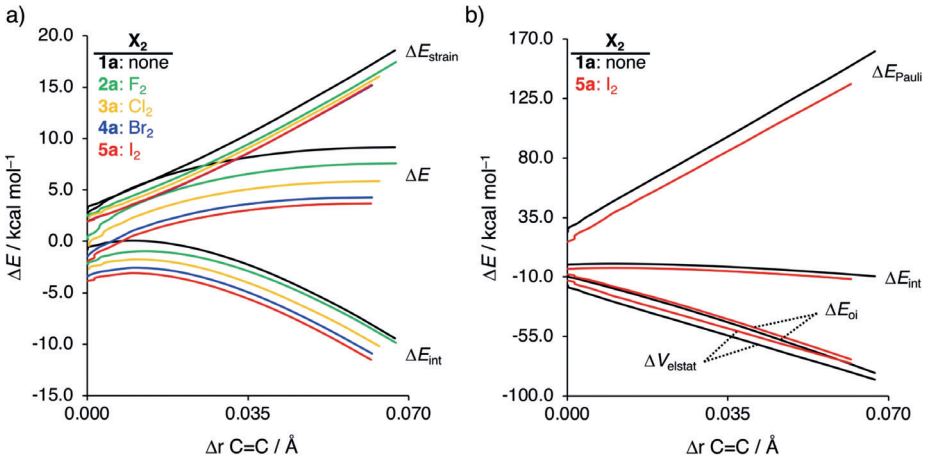


***Figure 2.*** a) Activation strain analyses of the Michael addition reactions between **py** and **1a**–**5a** and b) energy decomposition analyses of the least (**1a**, black lines) and most reactive (**5a**, red lines) substrates computed at the ZORA-M06-2X/TZ2P//M06-2X/def2-TZVP level.

the various features in the bonding mechanism.[11] Thus, the interaction $\Delta E_{int}$ between the reactants is further decomposed into three energy terms that can be associated with the following physical factors: classical electrostatic interaction ($\Delta V_{elstat}$), Pauli repulsive orbital interactions ($\Delta E_{Pauli}$) between closed-shell orbitals (actually, between same-spin electrons) which is responsible for steric repulsion,[15] and stabilizing orbital attractions ($\Delta E_{oi}$) that account, among others, for HOMO–LUMO interactions. For the purpose of clarity, only the corresponding energy decomposition analysis (EDA) results for the uncatalyzed (1) and $I_2$-catalyzed (5) reactions are shown in Figure 2b as these reactions represent the slowest and fastest reactions, respectively. Quite unexpectedly, we find that the process involving **5a** goes with a stronger interaction energy due exclusively to a much less destabilizing Pauli repulsion as compared to that involving **1a**. Indeed, both the electrostatic and orbital interactions in the process involving **5a** are even less stabilizing (not more stabilizing as one might have expected) than those for the reaction involving **1a**, despite the former exhibiting a more favorable (smaller) donor–acceptor FMO energy gap.

Clearly, the $\Delta E_{Pauli}$ term determines the trend in interaction energies and, ultimately, in activation barriers for these reactions. This finding is unprecedented and constitutes a novel physical mechanism behind the catalytic role of dihalogen molecules in the studied Michael addition reactions.[16]

To understand the origin of the less destabilizing Pauli repulsion for the $I_2$-catalyzed reaction, which results in the most favorable interaction energy and thus the lowest activation barrier of all the studied reactions, we performed a Kohn–Sham molecular orbital (KS-MO) analysis.[17] We have quantified the most significant four-electron interactions between filled molecular orbitals[18] of pyrrolidine (**py**) with **1a**–**5a** at consistent geometries with a C=C bond length stretch of 0.062 Å (Figure 3a). Analysis at a consistent point on the reaction coordinate, that is both close in geometry and energy to the actual TS, rather than at the transition state alone, ensures that the results are not skewed by the position

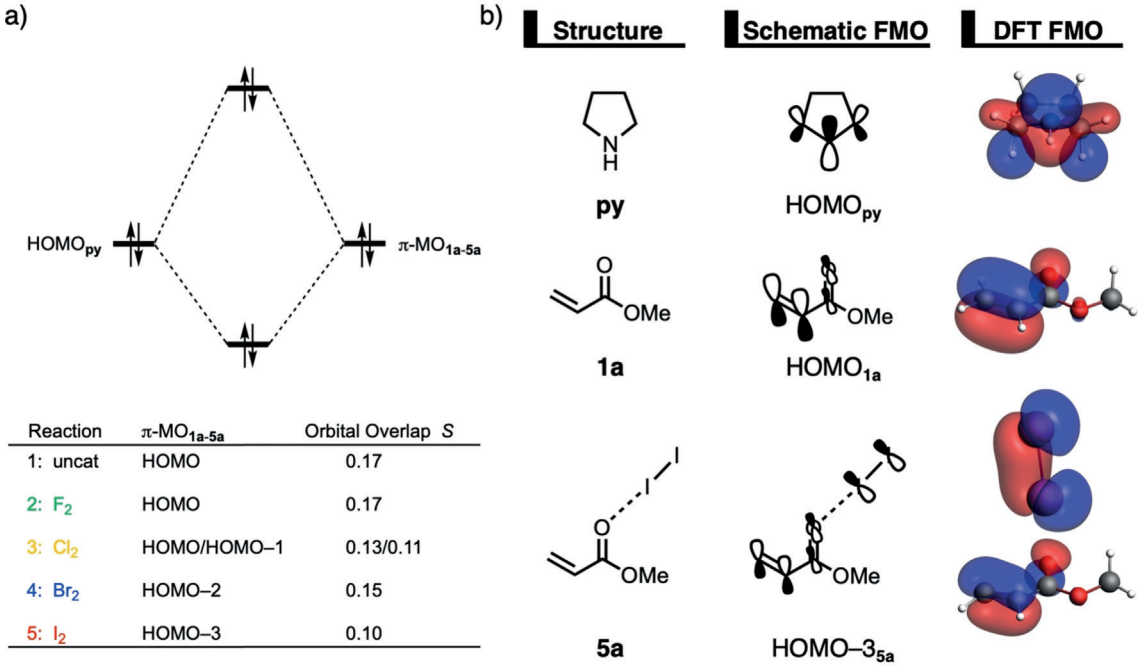


| Reaction | π-$MO_{1a-5a}$ | Orbital Overlap *S* |
|---|---|---|
| 1: uncat | HOMO | 0.17 |
| 2: $F_2$ | HOMO | 0.17 |
| 3: $Cl_2$ | HOMO/HOMO–1 | 0.13/0.11 |
| 4: $Br_2$ | HOMO–2 | 0.15 |
| 5: $I_2$ | HOMO–3 | 0.10 |

***Figure 3.*** a) Molecular orbital diagram and the most significant occupied orbital overlaps of the Michael addition reactions between **1a** and **5a** with **py** and b) key occupied orbitals (isovalue = 0.07) computed at the ZORA-M06-2X/TZ2P//M06-2X/def2-TZVP level.

  

of the transition state.[13] The π-$MO_{1a-5a}$ involved in this four-electron interaction is the HOMO for reactions 1 and 2, the HOMO and HOMO−1 for 3, the HOMO−2 for 4, and the HOMO−3 for 5. For the heavier dihalogens in **4a** and **5a**, the $X_2$ lone pairs are higher-lying[19] than the key π-FMO in **1a**, and for this reason, the π-MO in the adducts is lower in energy than the HOMO. The orbital overlap between the π-$MO_{1a-5a}$ and lone pair π-$HOMO_{py}$ is largest and most destabilizing for the uncatalyzed reaction (1) ($S = 0.17$) and smallest and least destabilizing for the $I_2$-catalyzed reaction (5) ($S = 0.10$) (see Figure 3b for the involved MOs). The polarization of the π-$MO_{2a-5a}$ away from the C=C double bond by the dihalogen is the reason for the decreased $HOMO_{py}|\pi\text{-}MO_{2a-5a}$ overlap. Weak, but non-negligible, donor–acceptor interactions between the σ*-$X_2$ and the π-HOMO of methyl acrylate (see Table 1) cause charge transfer from methyl acrylate to the $X_2$ moiety and results in less amplitude on the carbon atom directly involved in the Michael addition (schematically illustrated in Scheme 2). This follows from the expected trend of Lewis acidity of halogen atoms along the series F > Cl > Br > I.[20] Thus, the extent of polarization induced by the halogen is almost negligible for **2a**, but is more significant for **5a** as clearly viewed when comparing the corresponding π-density of the C=C bond (see Figure 3b).

We finally explored our counterintuitive EDA finding that the strength of the orbital interactions actually become weaker for the $I_2$-catalyzed (5) reaction than for the uncatalyzed (1) reaction, although the former exhibits a more favorable FMO energy gap. We have computed the frontier molecular orbital (FMO) gaps and overlaps, once again, on consistent geometries with a C=C bond length stretch of 0.062 Å (Figure 4). As expected, the FMO energy gaps for the $HOMO_{py}$–$LUMO_{1a-5a}$ interaction decrease and range from 6.1 to 5.4 eV for the uncatalyzed and the $I_2$-catalyzed reaction, respectively. Despite the more favorable FMO gaps, the strength of the orbital interactions actually becomes less stabilizing for the $X_2$-catalyzed reactions due to poorer orbital overlap. The computed orbital overlap decreases significantly from $S = 0.19$ to 0.13 for reactions 1 and 5, respectively. There are two FMO interactions for reaction 4 that involve both the nearly degenerate $LUMO_{4a}$ ($S = 0.10$) and $LUMO+1_{4a}$ ($S = 0.15$) virtual π* orbitals. Thus, it is the poorer FMO orbital overlaps that arise, again, from the polarization of the LUMO away from the C=C double bond by the dihalogen. This polarization-induced weakening of the FMO orbital overlaps effectively counteracts the more favorable (smaller) energy gaps and results in less stabilizing orbital interactions when descending Group 17 for the $X_2$.

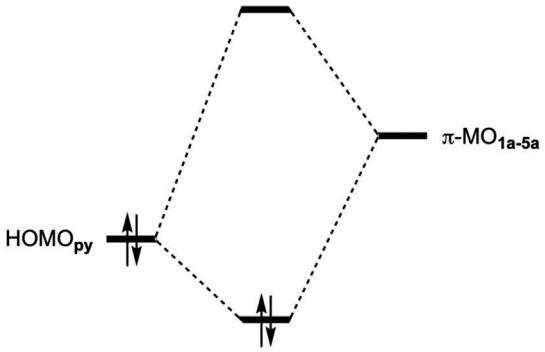


| Reaction | Δε $HOMO_{py}$–π-$MO_{1a-5a}$ (eV) | | Orbital Overlap *S* |
|---|---|---|---|
| 1: uncat | LUMO | 6.1 | 0.19 |
| 2: $F_2$ | LUMO | 6.0 | 0.17 |
| 3: $Cl_2$ | LUMO | 5.8 | 0.14 |
| 4: $Br_2$ | LUMO | 5.4 | 0.10 |
| | LUMO+1 | 6.1 | 0.15 |
| 5: $I_2$ | LUMO | 5.4 | 0.13 |

***Figure 4.*** Molecular orbital diagram with the orbital energy gap and overlap of the $HOMO_{py}$-π-$MO_{1a-5a}$ interaction for the Michael addition reactions 1–5 computed at the ZORA-M06-2X/TZ2P//M06-2X/def2-TZVP level.

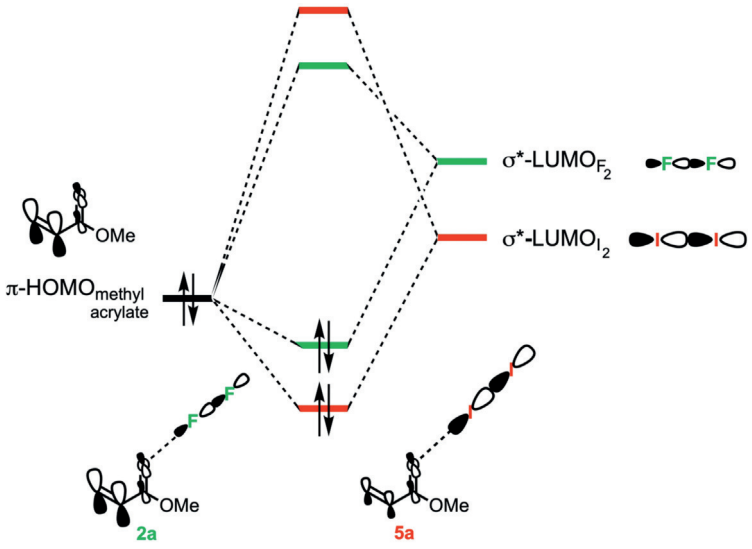


***Scheme 2.*** Schematic orbital interaction diagram between the π-HOMO of methyl acrylate and the σ*-LUMO of $X_2$ for **2a** ($X_2 = F_2$) and **5a** ($X_2 = I_2$) resulting in a smaller amplitude of the resulting π orbital on the terminal carbon atom involved in the forming C–N bond.

In conclusion, our ASM-EDA study shows that the dihalogen catalysis of the considered Michael additions is brought about by a hitherto unknown electronic mechanism: we find that it is not caused by an effective enhancement of the Lewis acidity of the Michael acceptor leading to an enhanced donor–acceptor [HOMO(nucleophile)–LUMO(Michael acceptor)] interaction. Instead, the decrease in barrier when $X_2$ binds to the carbonylic oxygen of the Michael acceptor is due to the concomitant polarization of its conjugated π-system away from the electrophilic carbon atom. This has the effect of reducing the four-electron (Pauli) repulsion with the lone pair of the nucleophile. This reduction in repulsion causes an en-

  

hancement of the overall nucleophile–Michael acceptor interaction and thus the observed lowering of the reaction barrier.

## Acknowledgements

This work was supported by the Netherlands Organization for Scientific Research (NWO) and the Spanish MINECO (CTQ2016-78205-P and CTQ2016-81797-REDC).

## Conflict of interest

The authors declare no conflict of interest.

**Keywords:** activation strain model · density functional calculations · halogen bonding · Michael addition · Pauli repulsion · reactivity

**How to cite:** *Angew. Chem. Int. Ed.* **2019**, *58*, 8922–8926
*Angew. Chem.* **2019**, *131*, 9015–9020

[1] a) A. Michael, *J. Prakt. Chem.* **1887**, *35*, 349; b) A. Michael, *J. Prakt. Chem.* **1894**, *49*, 20. See also: T. Tokoroyama, *Eur. J. Org. Chem.* **2010**, 2009.

[2] a) E. D. Bergmann, D. Ginsburg, R. Pappo, *Org. React.* **1959**, *10*, 179; b) P. Perlmutter, *Conjugate Addition Reactions in Organic Synthesis*, Pergamon, Oxford, **1992**.

[3] For selected reviews on asymmetric Michael additions, see: a) N. Krause, H. Roder, *Synthesis* **2001**, 0171; b) O. M. Berner, L. Tedeschi, D. Enders, *Eur. J. Org. Chem.* **2002**, 1877; c) J. Christoffers, A. Baro, *Angew. Chem. Int. Ed.* **2003**, *42*, 1688; *Angew. Chem.* **2003**, *115*, 1726; d) J. L. Vicario, D. Badía, L. Carrillo, J. Etxebarria, E. Reyes, N. Ruiz, *Org. Prep. Proced. Int.* **2005**, *37*, 513; e) Y. Zhang, W. Wang, *Catal. Sci. Technol.* **2012**, *2*, 42; f) K. M. Byrd, *Beilstein J. Org. Chem.* **2015**, *11*, 530; g) D. A. Alonso, A. Baeza, R. Chinchilla, C. Gómez, G. Guillena, I. M. Pastor, D. J. Ramón, *Molecules* **2017**, *22*, 895.

[4] Selected representative examples: a) M. Kurosu, L. R. Marcin, T. J. Grinsteiner, Y. Kishi, *J. Am. Chem. Soc.* **1998**, *120*, 6627; b) H. Masaki, J. Maeyama, K. Kamada, T. Esumi, Y. Iwabuchi, S. Hatakeyama, *J. Am. Chem. Soc.* **2000**, *122*, 5216; c) L. A. Paquette, J. Tae, M. P. Arrington, A. H. Sadoun, *J. Am. Chem. Soc.* **2000**, *122*, 2742; d) E. J. Corey, F.-Y. Zhang, *Org. Lett.* **2000**, *2*, 1097; e) Z. Dong, L. Wang, X. Chen, X. Liu, L. Lin, X. Feng, *Eur. J. Org. Chem.* **2009**, 5192; f) J. Hu, M. bian, H. Ding, *Tetrahedron Lett.* **2016**, *57*, 5519.

[5] See, for instance: a) G. Sengle, A. Eisenfür, P. Arora, J. Nowick, M. Famulok, *Chem. Biol.* **2001**, *8*, 459; b) A. Dinkova-Kostova, M. Massiah, R. Bozak, R. Hicks, P. Talalay, *Proc. Natl. Acad. Sci. USA* **2001**, *98*, 3404.

[6] Representative examples: a) C.-M. Chu, S. Gao, M. N. V. Sastry, C.-F. Yao, *Tetrahedron Lett.* **2005**, *46*, 4971; b) C. Lin, J. Hsu, M. N. V. Sastry, H. Fang, Z. Tu, J.-T. Liu, Y. Ching-Fa, *Tetrahedron* **2005**, *61*, 11751; c) L. Wu, B. Niu, W. Li, F. Yan, *Bull. Korean Chem. Soc.* **2009**, *30*, 2777; d) K. J. Borah, M. Phukan, R. Borah, *Synth. Commun.* **2010**, *40*, 2830.

[7] See, for instance: a) J. Zhang, D. Zhu, C. Yu, C. Wan, Z. Wang, *Org. Lett.* **2010**, *12*, 2841; b) M. Jereb, D. Vražič, M. Zupan, *Tetrahedron* **2011**, *67*, 1355; c) Y.-M. Ren, C. Cai, R.-C. Yang, *RSC Adv.* **2013**, *3*, 7182; d) G. Satish, *Synlett* **2015**, *26*, 1913.

[8] Selected theoretical studies: a) M. Yasuda, K. Chiba, N. Ohigashi, Y. Katoh, A. Baba, *J. Am. Chem. Soc.* **2003**, *125*, 7291; b) D. C. Chatfield, A. Augsten, C. D′Cunha, E. Lewandowska, S. F. Wnuk, *Eur. J. Org. Chem.* **2004**, 313; c) M. J. Zhou, Y. Li, L. Dang, *Asian J. Org. Chem.* **2015**, *4*, 904; d) C. Giraldo, S. Gómez, F. Weinhold, A. Restrepo, *ChemPhysChem* **2016**, *17*, 2022.

[9] a) M. Breugst, E. Detmar, D. von der Heiden, *ACS Catal.* **2016**, *6*, 3203; b) D. Von der Heiden, S. Bozkus, M. Klussmann, M. Breugst, *J. Org. Chem.* **2017**, *82*, 4037. For a related study involving pnicogen bonding, see: c) J. Schmauck, M. Breugst, *Org. Biomol. Chem.* **2017**, *15*, 8037.

[10] All stationary points in this study were located at the M06-2X-def2-TZVP level. All activation strain and energy decomposition analyses were computed at the ZORA-M06-2X/TZ2P//M06-2X-def2-TZVP level. See the Supporting Information for all computational details and Table S3 for Cartesian coordinates of all stationary points.

[11] a) L. Zhao, M. von Hopffgarten, D. M. Andrada, G. Frenking, *WIRES Comput. Mol. Sci.* **2018**, *8*, e1345; b) F. M. Bickelhaupt, A. Diefenbach, S. P. de Visser, L. J. de Koning, N. M. M. Nibbering, *J. Phys. Chem. A* **1998**, *102*, 9549; c) F. M. Bickelhaupt, N. M. M. Nibbering, E. M. van Wezenbeek, E. J. Baerends, *J. Phys. Chem.* **1992**, *96*, 4864; d) T. Ziegler, A. Rauk, *Inorg. Chem.* **1979**, *18*, 1558.

[12] a) G. S. Hammond, *J. Am. Chem. Soc.* **1955**, *77*, 334; b) A. Pross, *Theoretical and Physical Principles in Organic Reactivity*, Wiley, Hoboken, **1995**.

[13] a) F. M. Bickelhaupt, K. N. Houk, *Angew. Chem. Int. Ed.* **2017**, *56*, 10070; *Angew. Chem.* **2017**, *129*, 10204; b) L. P. Wolters, F. M. Bickelhaupt, *WIRES Comput. Mol. Sci.* **2015**, *5*, 324; c) I. Fernández, F. M. Bickelhaupt, *Chem. Soc. Rev.* **2014**, *43*, 4953; d) W.-J. van Zeist, F. M. Bickelhaupt, *Org. Biomol. Chem.* **2010**, *8*, 3118; e) F. M. Bickelhaupt, *J. Comput. Chem.* **1999**, *20*, 114.

[14] The reaction coordinate can be equally projected onto the forming C···N bond and the reactivity trends are nearly identical (see Figure S3 in the Supporting Information).

[15] The Pauli repulsion term, $\Delta E_{\text{Pauli}}$, is computed in the EDA scheme by antisymmetrization of the Hartree wavefunction, that is, the product of frozen fragment wavefunctions, which leads to an increase in the kinetic energy of the electrons. See Table S2 in the Supporting Information for the numerical output from an energy decomposition analysis calculation in ADF used to compute the Pauli repulsion along with the other energy terms.

[16] Pauli repulsion has been found to be decisive in other transformations such as Diels–Alder cycloadditions, acetylene trimerization, and $S_N2$ reactions. See, for instance: a) Y. García-Rodeja, M. Solà, I. Fernández, *Phys. Chem. Chem. Phys.* **2018**, *20*, 28011; b) S. Yu, H. M. de Bruijn, D. Svatunek, T. A. Hamlin, F. M. Bickelhaupt, *ChemistryOpen* **2018**, *7*, 995; c) M. A. van Bochove, M. Swart, F. M. Bickelhaupt, *J. Am. Chem. Soc.* **2006**, *128*, 10738.

[17] a) F. M. Bickelhaupt, E. J. Baerends, in *Reviews in Computational Chemistry* (Eds.: K. B. Lipkowitz, D. B. Boyd), Wiley, Hoboken, **2000**, pp. 1–86; b) R. van Meer, O. V. Gritsenko, E. J. Baerends, *J. Chem. Theory Comput.* **2014**, *10*, 4432.

[18] T. A. Albright, J. K. Burdett, M. H. Whangbo, *Orbital Interactions in Chemistry*, 2nd ed, Wiley, Hoboken, **2013**.

[19] W. L. Jolly, C. J. Eyermann, *Inorg. Chem.* **1983**, *22*, 1566.

[20] D. P. N. Satchell, R. S. Satchell, *Q. Rev. Chem. Soc.* **1971**, *25*, 171.

Manuscript received: March 14, 2019
Revised manuscript received: April 4, 2019
Accepted manuscript online: April 29, 2019
Version of record online: May 24, 2019

  